

Article

The Experimentally Measured Influence of the Si-MOSFET Replacement Switches to WBG Transistors in the Voltage Source Inverters as the Source of Radiation Noise

Krzysztof Bernacki  and Zbigniew Rymarski * 

Department of Electronics, Electrical Engineering and Microelectronics, Faculty of Automatic Control, Electronics and Computer Science, Silesian University of Technology, Akademicka 16, 44-100 Gliwice, Poland; krzysztof.bernacki@polsl.pl

* Correspondence: zbigniew.rymarski@polsl.pl; Tel.: +48-602662249

Abstract: The aim of the paper is to present the change in the radiation noise of the single-phase voltage source inverter (VSI) when the Si-MOSFET transistors are replaced by the wide-band-gap (WBG) SiC-MOSFET and GaN transistors. The power spectral density of the near-field interference is used to visualise the change of the radiation noise of the VSI. The conclusions concern the results of the experimental replacement of the switches to the WBG technology in the existing inverters. Three switching frequencies and two gate circuits were used to show the change in the radiation noise. The measurements of the experimental VSI are presented.

Keywords: voltage source inverter; wide-band-gap transistors; near-field interferences; power spectral density; radiation noise



Citation: Bernacki, K.; Rymarski, Z. The Experimentally Measured Influence of the Si-MOSFET Replacement Switches to WBG Transistors in the Voltage Source Inverters as the Source of Radiation Noise. *Energies* **2023**, *16*, 870. <https://doi.org/10.3390/en16020870>

Academic Editor: Miguel Castilla

Received: 22 November 2022

Revised: 14 December 2022

Accepted: 10 January 2023

Published: 12 January 2023



Copyright: © 2023 by the authors. Licensee MDPI, Basel, Switzerland. This article is an open access article distributed under the terms and conditions of the Creative Commons Attribution (CC BY) license (<https://creativecommons.org/licenses/by/4.0/>).

1. Introduction

The voltage source inverters (VSI) work in the switching mode. It always produces all the types of disturbances that depend on the pulse slope increase or decrease speed, the switched current, and the switched PWM voltage amplitude. Different types of semiconductor power switches can be used. In the small and middle power converters (IEC 62040-3 [1] define the borders of measuring parameters methods to 3 kW or 4 kW), the Si-MOSFET enhancement-mode switches are the most often used. However, in the last years, they are replaced with the wide-band-gap (WBG) transistors or for the low drain to source voltages V_{DS} (about 30 V), a third-generation of macrocell power MOSFET technology recently introduced by Texas Instruments, NexFET™ technology, that offers a very low resistance $R_{DS(on)}$ of the open channel and low capacitances C_{gd} , which is very important because of the Miller effect during switching. In this paper, the GaN, SiC (WBG) technologies of transistors will be compared with the standard Si-MOSFET n-channel switches. It should be mentioned that the advantage of enhanced n-channel Si switches is the driving threshold voltage over zero and they are much cheaper than WBG transistors. The Si-MOSFET transistors require a “current attack” during switching on; however, the commercial drivers fill this requirement by giving over a very short current pulse to recharge the input capacitances of the transistor. For the inductive load (e.g., the output filter inductance) during loading the gate to source capacitance C_{gs} and, more significantly, the gate to drain capacitance C_{gd} when the Miller effect ([2,3]) exists, the power losses when MOSFET goes through the active region are significant. The static power losses on the $R_{DS(on)}$ resistance are the result of the vertical structure of the power MOSFET and are proportional to the maximum drain to source V_{DS} voltage—the higher V_{DS} the higher conducting channel resistance $R_{DS(on)}$. So, the goal of replacing the Si-MOSFET transistors with new WBG technology is the reduction of the reverse transfer capacitance $C_{rss} = C_{gd}$, the input capacitance $C_{iss} = C_{gs} + C_{gd}$, and the output capacitance $C_{oss} = C_{gd} + C_{ds}$ (C_{ds} is

not so important). The other parameter [2,4] that should be decreased is the gate charge Q_g ; however, the switching power losses are during loading the charge Q_{sw} (where $Q_{sw} < Q_g$, $Q_{sw} > Q_{gd}$). So, the basic parameters— R_{DSON} and C_{iss} (but, mainly C_{gd})—that are proportional to the charge Q_g (but, strictly to Q_{sw}) decide about the static and dynamic losses of the Si-MOSFET switch. WBG semiconductor devices appeared in the semiconductor market [5–8] in the last few years. The GaN and SiC technologies are presented in the paper. With every year, they were improved for easy replacement with Si-MOSFET. Now, they are produced in the enhanced-mode channel versions (an early problem with GaN that is solved through cascade hybrid transistors) with threshold voltages over zero (an early problem with SiC). The WBG transistors with the V_{DS} voltage of transistors equal to hundreds of volts have a much lower R_{DS} resistance and much lower internal capacitances. The typical high-electron-mobility GaN transistor (HEMT), also known as a heterostructure field-effect transistor (HFET) or modulation-doped FET (MODFET), were depletion channel transistors, inconvenient for control. That is why GaN HEMT with low voltage (very low R_{DSON} of the channel) Si-MOSFET is used in the cascode device structure operating together as a substitute for the enhancement channel transistor. HEMT is a field-effect transistor incorporating a junction between two materials with different bandgaps (i.e., a heterojunction) as the channel instead of a doped region. The main charge carriers in the HEMT transistor are the majority carriers, which results in its high speed. The possible reduced dead times in the inverter GaN HEMTs bridge make that the inverter can operate with a higher efficiency and a lower THD of the output VSI voltage. Low on-state resistance R_{DSON} and smaller capacitances compared to Si-MOSFETs make GaN HEMTs useful for high-speed switching power conversion.

The SiC technology offers a higher allowable junction temperature than Si. Owing to this, the SiC devices are predicted for automotive applications and industrial applications. The lower energy loss of the SiC technology during the reverse recovery phase (e.g., in the body diode of SiC-MOSFET) is one of their advantages (approximately 1% of the energy lost by Si technology). The SiC-MOSFET dissipates less energy and can switch at higher frequencies and improve efficiency. The SiC technology offers up to ten times higher dielectric breakdown field strength, twice higher electron saturation velocity, triple higher energy bandgap, and triple higher thermal conductivity than Si devices. The SiC-MOSFET advantages include high efficiency of the power conversion by lowering power loss, greater power density, higher operating frequency, and increased temperature range operation. Initially, SiC-MOSFETs required the negative gate driving voltage for off-state (for n-channel), which disable the simple exchange with Si-MOSFETs, now SiC-MOSFETs, with a positive threshold voltage being present on the market.

The possibility of exchanging the Si-MOSFETs in the existing inverter project for the WBG transistors present on the market is an important designer problem. The first problem is about the 5 to 10 times higher price of the WBG transistors with a similar VDS voltage than the price of the Si-MOSFET. However, in some projects, the higher efficiency is worth it. The other problem is the control system. It is designed to take into care the higher equivalent serial resistance of the inverter with the Si-MOSFETs bridge than for the WBG transistors bridge. In [9], the possibility of simply replacing the old Si-MOSFET on GaN and SiC transistors concerning the control system was discussed. It was presented that for multi-input single-output (MISO) control by measuring the output voltage, the output current and the inductor current in the exemplary passivity based control (PBC) [10–14] decreasing the equivalent serial resistance does not influence the maximum voltage and current gains of the control system [9]. So, the exchange is possible without adjusting the control. On the contrary, when using the single-input single-output (SISO) control [15–19], the influence of the decreasing the equivalent serial resistance is noticeable; in addition, in the case of the exemplary coefficient diagram method for the low order (the second order) of the nominator and denominator of the controller transfer function, this can cause instability. In the case of the higher order of the controller transfer function, the improper setting of the equivalent serial resistance of the inverter in the control law leads to the

higher total harmonic distortion (THD) of the output voltage [9]; for example, the nonlinear rectifier RC load [1]. The equivalent serial resistance of the inverter depends on the many elements, e.g., the power losses in the core of the output filter coil [20–22]; however, we discuss the case when all these factors are the same (switching frequency, the core magnetic material, the PCB layout), while only switching transistors are changed from Si-MOSFETs to WBG transistors.

The lower input capacitances and shorter switching slopes for WBG transistors make that transistor's gate driving circuits for Si-MOSFETs; this can be a reason for the oscillations after changing transistors. WBG transistors can oscillate owing to the associated parasitic elements, e.g., the imperfect PCB layout. Switching oscillations can be damped using RC snubbers, ferrite beads, the reduction of di/dt or novel gate driver designs [23]. Too long a trace designed in a printed circuit board (PCB) between the gate driver output and the gate-source terminal leads to a high parasitic inductance in the gate loop and can damage the SiC transistor [24]. What is more, the SiC MOSFET is sensitive even to parasitics in the measurement probe and measuring; e.g., the gate-source voltage can introduce the parasitic inductance between the test point and the ground lead of the probe, and as the result decrease the stability of SiC MOSFET [25]. The simplest solution is adding the higher serial resistor in the gate circuit; if for the previously designed PCB for the Si-MOSFETs bridge, we notice the drain-source oscillations after exchange to WBG transistors. However, it makes the slower drain to source voltage increase/decrease and the higher dynamic power losses.

The electromagnetic compatibility (EMC) of the VSI depending on the PWM schema was presented in [26] and the EMC of VSI with the impedance networks in [27]. The aim of this paper is the experimental comparative checking of the radiation noise of the single-phase VSI when changing Si-MOSFET to SiC-MOSFET and the GaN&Si-MOSFET cascode device structure. The simplest way for the comparison is measuring near-field interference [28,29] on the gate, drain, and source of the chosen transistor from the bridge. The most useful is the measurement of the source of one of the high transistors in the bridge when using so-called the first modulation scheme [26] (Figure 1 where the output switching frequency is the double transistors switching frequency f_s).

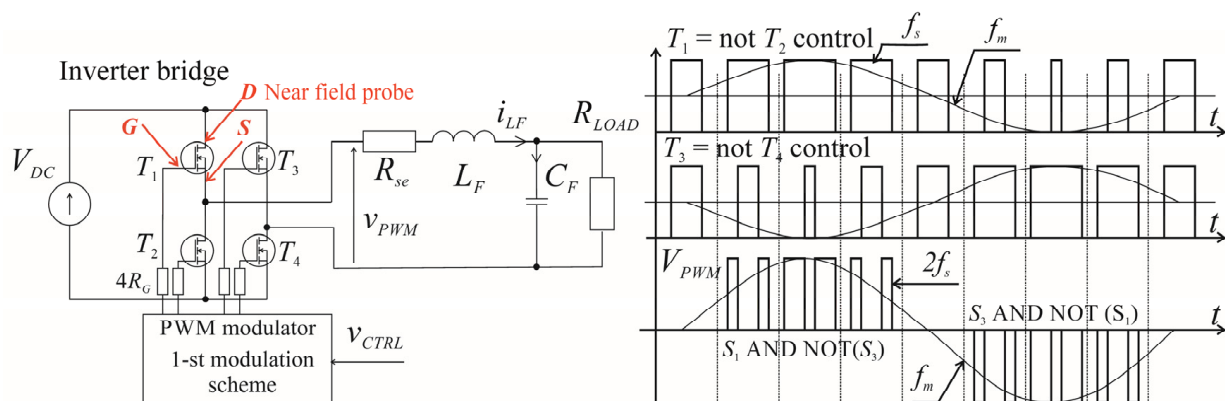


Figure 1. The block diagram of the tested VSI and the control waveforms.

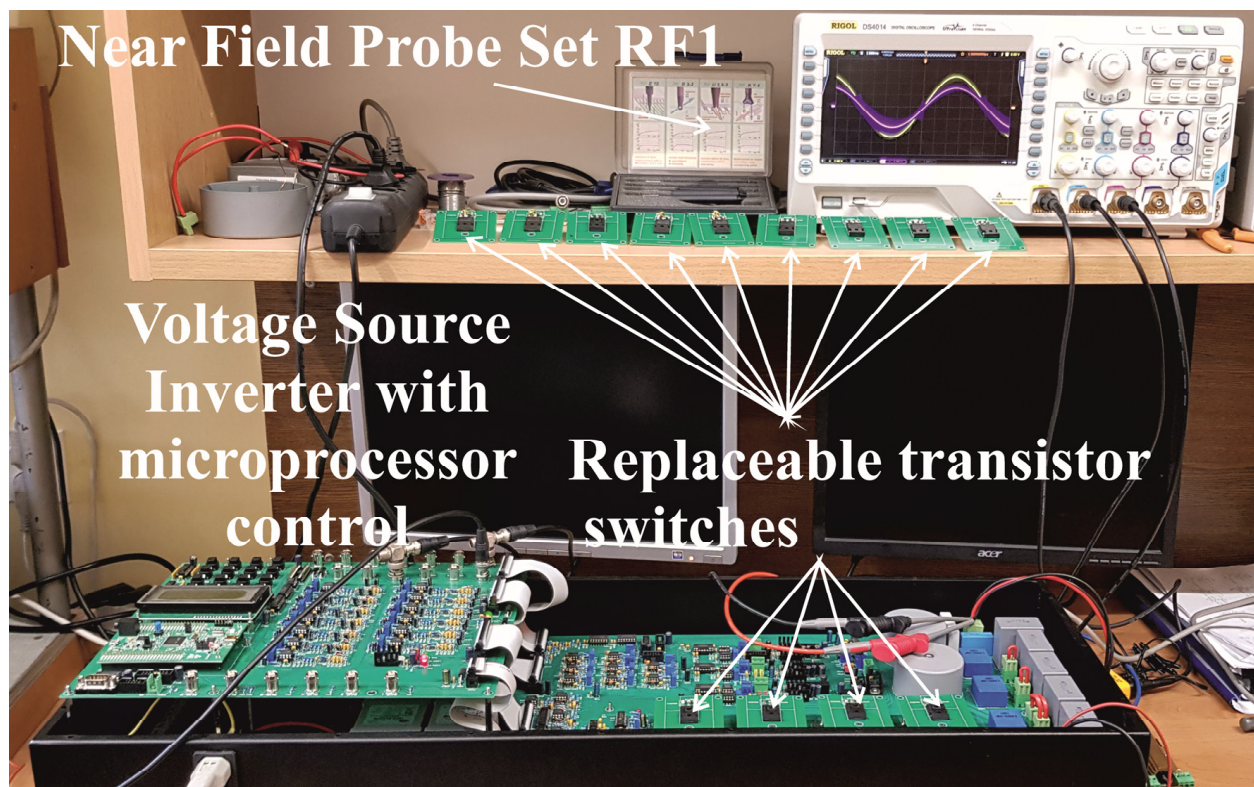
The serious impact on the near field interference can have the serial resistance R_G in the gate circuit (it will be discussed). Section 2 presents the methods of the measurement of near-field interference. Section 3 is a comparative presentation of the measurement results. Section 4 presents the results of the measurements and Section 5 contains conclusions. The basic static and dynamic properties of the tested Si, SiC, and GaN transistors are presented in Table 1.

Table 1. Basic properties of the tested transistors.

	V_{DS} [V], I_D [A]	R_{DS} [m Ω] ($T_j = 25^\circ\text{C}$) ($V_{GS} = 10\text{ V}, I_D = 14\text{ A}$)	$C_{iss}, C_{oss}, C_{rss}$ [pF] ($V_{GS} = 0\text{ V}, f = 1.0\text{ MHz}$) ($V_{DS} = 25\text{ V}$)
Standard Si-MOSFET IRFP360 (Vishay)	400 V, 23 A	200 ($V_{GS} = 10\text{ V}, I_D = 14\text{ A}$)	4500, 1100, 490 ($V_{DS} = 25\text{ V}$)
GaN + Si-MOSFET Cascode device structure GAN041-650WSB	650 V, 47.2 A	35 ($V_{GS} = 10\text{ V}; I_D = 32\text{ A}$)	1500, 147, 5 ($V_{DS} = 400\text{ V}$)
SiC-MOSFET AIMW120R060M1H	1200 V, 36 A	60 ($V_{GS} = 18\text{ V}, I_D = 13\text{ A}$)	1060, 58, 6.5 ($V_{DS} = 800\text{ V}$)

2. Methods of the Near-Field Interference Measurement of the Inverter

The experimental model of the voltage source inverter (VSI) with the replaceable transistors and possibility of changing the serial resistors in the gate circuit, inserted in the open iron box is presented in Figure 2.

**Figure 2.** The experimental model with the replaceable transistors.

The experimental model of VSI (100 V, 1 A) operated with the switching frequency $f_s = 12,800, 25,600$ and $51,200$ Hz with a filter with inductor with a super MSS core $L_F = 2$ mH and MKP capacitor $C_F = 50$ μF ; the resistive load $50\ \Omega$. It worked with the most commonly used first schema [26,30] of the 3-level, double-edge PWM modulation (Figure 1). This schema of modulation results in the double $2f_s$ transistor switching frequency f_s in the output filter and the load. It helps to reduce the filter inductor value and this type of PWM scheme enables the precise control of the output voltage when crossing zero. It is expected that the higher interferences will be generated on the source pin of the T_1 (or T_3) or drain of T_2 (or T_4) transistors where there is the highest change of voltage with the double switching frequency. However, the double switching frequency of the transistor current makes the

interference generated on the drain and source not so different (5 dB). The interferences generated on the source, gate, and the drain of T_1 were measured for two values (10 and 30 Ω) of the R_G resistors (protecting transistors from oscillations). The experimental comparative measurements of the Si-MOSFET, GaN-hybrid, and SiC-MOSFET (Table 1) were presented and discussed. The near-field interferences (NFI) depend on the many features of the VSI including PCB layout; so, only comparative measurements in the same VSI can give valuable data. The near field probe RF U 2, 5-2 with the bandpass up to 3 GHz from the near-field probe set RF 1, AFJ International SRL for NFI measurements were used.

The 14,000,000 samples of the NFI time-dependent waveform during 28 ms were collected in the Siglent SDS 1104X-E 100 MHz digital oscilloscope. So, the sampling period was 2 ns and the sampling frequency was 500 MHz. In the result of the Fourier transform, the harmonics up to 250 MHz were measured, which is a sufficient range (taking into care the damping of harmonics over about 50 MHz). The simple FFT analysis gives unclear results. That is why the power spectral density—the distribution of power into frequency components composing the measured NFI signal—was used [31,32]. The measured VSI had switching frequencies $f_s = 12,800$ Hz, 25,600 Hz and 51,200 Hz. The resolution $2 f_s$ of the power spectral density in the MATLAB “pspectrum” function was used because the load current and voltage have the double switching frequency. To protect the analyzed data against frequency leakage, the Blackman window that has better than the Hamming window stop band attenuation and advised for the collected samples in [30] was implemented.

3. The Comparative Analysis of the Power Spectral Density of the Near-Field Interferences

The near-field interferences were measured at the drain, gate, and source pins of the T_1 transistor that was replaced between Si-MOSFET, GaN-hybrid, and SiC-MOSFET for two-gate resistor values R_G equal to 10 and 30 Ω . For $f_s = 12,800$ Hz, the power spectral density characteristics of the NFI on the pins of T_1 from Figure 1 are presented in Figure 3, for $f_s = 25,600$ Hz in Figure 4, and $f_s = 51,200$ Hz in Figure 5. The NFI at the source of T_1 for all the switching frequencies and two R_G values is presented in Figure 6.

The highest power spectral density of NFI is on the source of T_1 from Figures 2 and 6, and presents the comparison between NFI (Table 2) in this place. The measurements of the power spectral density present that near-field interferences have three or four (for GaN only) local maxima—below $2 f_s$, the range 2.4–3.4 MHz, the range 23–24 MHz (for GaN only), and the range 29–35 MHz. For the low frequency, the gate resistor R_G damps interferences on the source of Si and SiC transistors from -36 dB to -56 dB; however, the interferences of the source of the GaN transistor stay on the same level. For the range 2.5–3.3 MHz, the highest interferences are for Si transistors and they do not seriously depend on the gate resistor. For the 23–24 MHz range, only the GaN source has the local NFI maximum and for 29–35 MHz, the highest interferences are for the GaN transistor. The conclusion for the measurements of NFI is such that for the same f_s , the increase of R_G from 10 to 30 Ω reduces the power spectral density of NFI over 20 dB in the case of Si-MOSFET and SiC-MOSFET transistors and does not influence the GaN transistor in the case of low-frequency NFI for $f < 2 f_s$. For the two higher ranges of frequency, the influence of increasing R_G is not noticeable (up to -2 dB). Interestingly, the GaN-hybrid transistor has two local maxima of NFI in the 23–24 MHz and 34–35 MHz ranges, probably owing to two internal transistors, while Si and SiC transistors have only a single maximum in this range (29–35 MHz). The power spectral density of the NFI difference between different types of transistors in the range over 2.5 MHz is not higher than 10 dB. Over 50 MHz, the power spectral density of NFI is about -90 – -100 dB and is not considered (power spectral density is measured in the range up to 250 MHz). Doubling the switching frequency causes a 2–10 dB increase of NFI in two higher ranges of frequency.

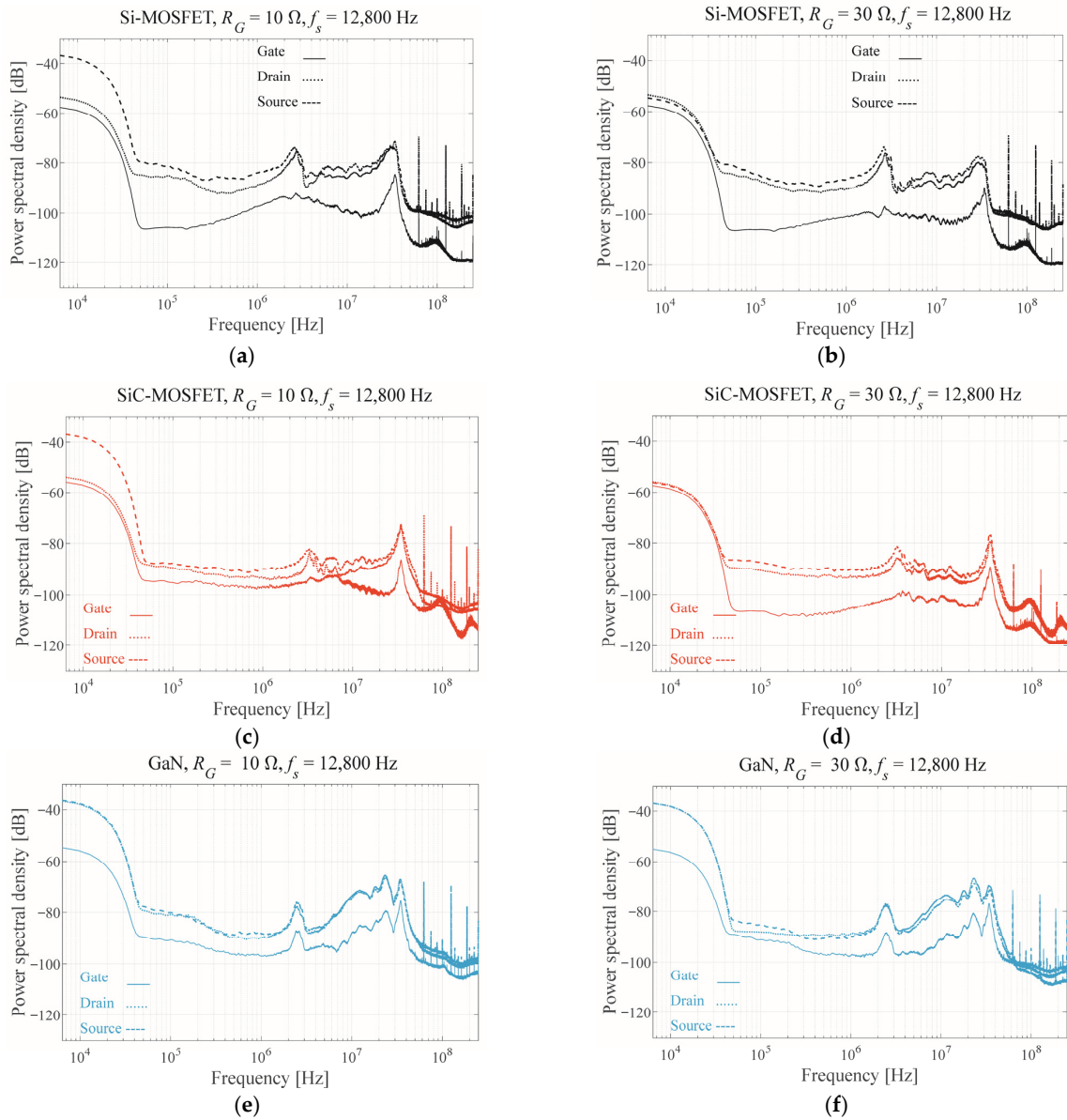


Figure 3. The power spectral density [dB] of the near-field interferences for Si, SiC, and GaN T_1 transistors for $f_s = 12,800$ Hz: (a) Si, $R_G = 10 \Omega$; (b) Si, 30Ω ; (c) SiC, 10Ω ; (d) SiC, 30Ω ; (e) GaN, 10Ω ; (f) GaN, 30Ω .

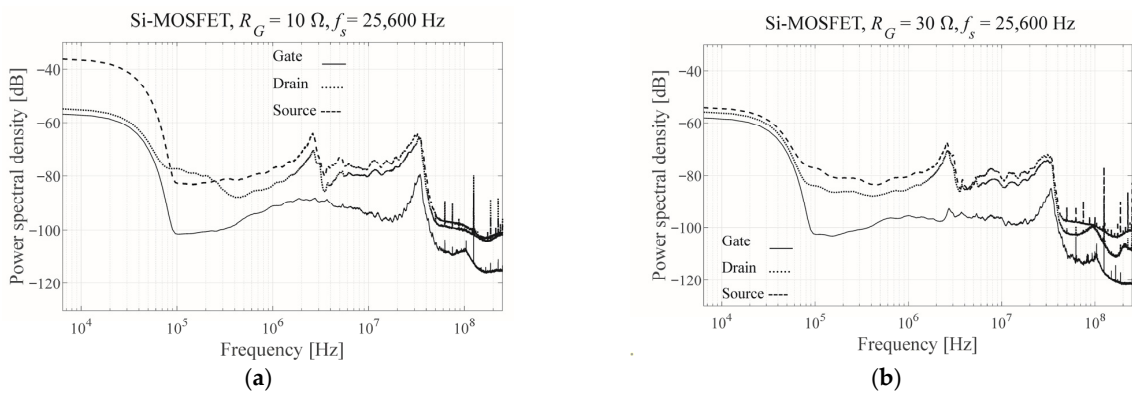


Figure 4. Cont.

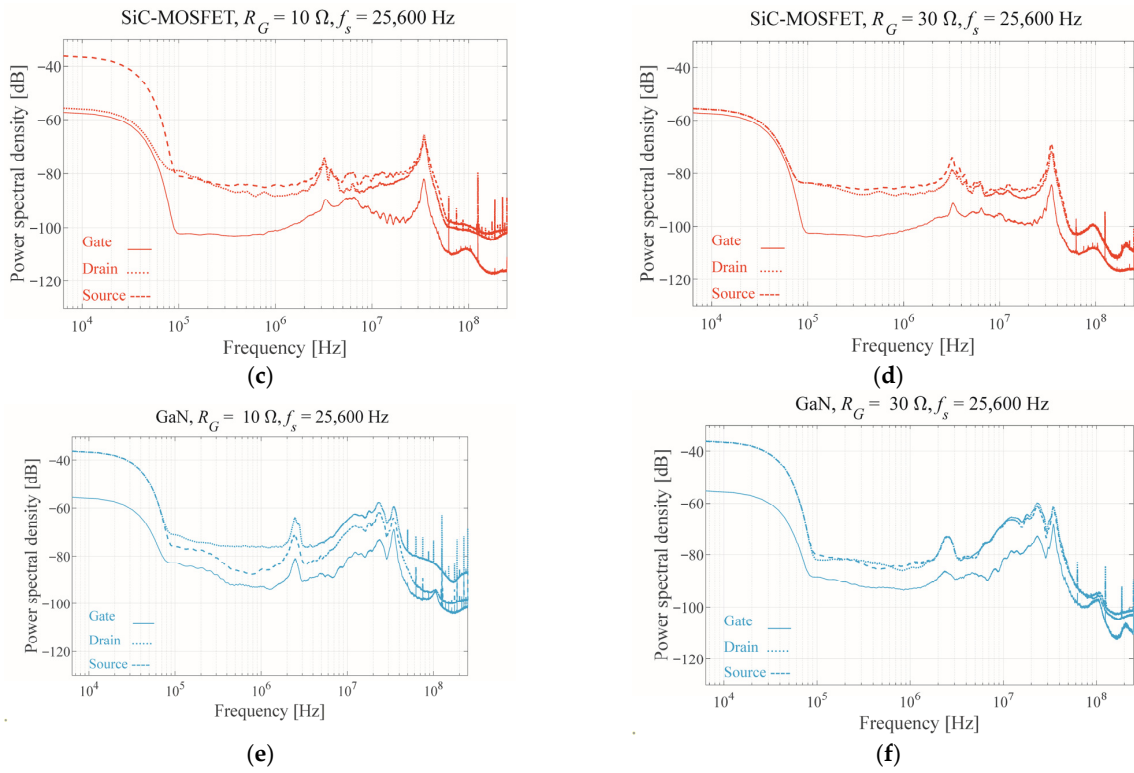


Figure 4. The power spectral density [dB] of the near-field interferences for the Si, SiC, and GaN T_1 transistors for $f_s = 25,600$ Hz: (a) Si, $R_G = 10 \Omega$; (b) Si, 30Ω ; (c) SiC, 10Ω ; (d) SiC, 30Ω ; (e) GaN, 10Ω ; (f) GaN, 30Ω .

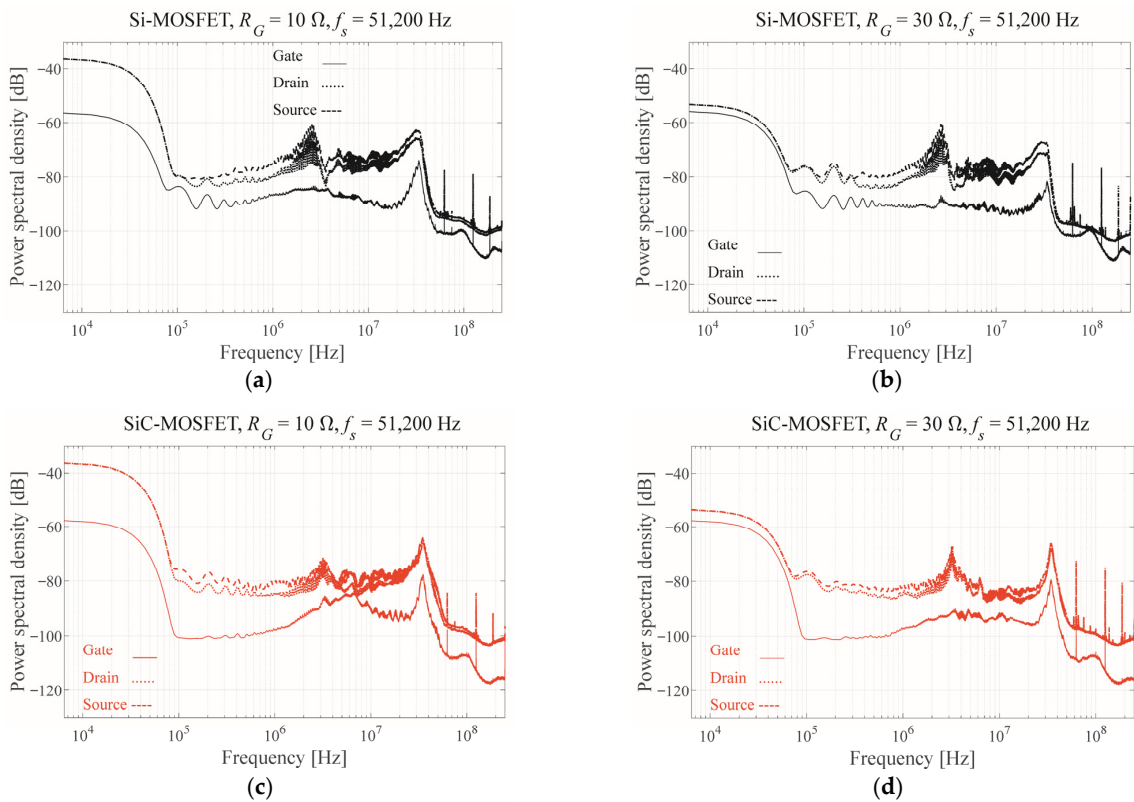


Figure 5. Cont.

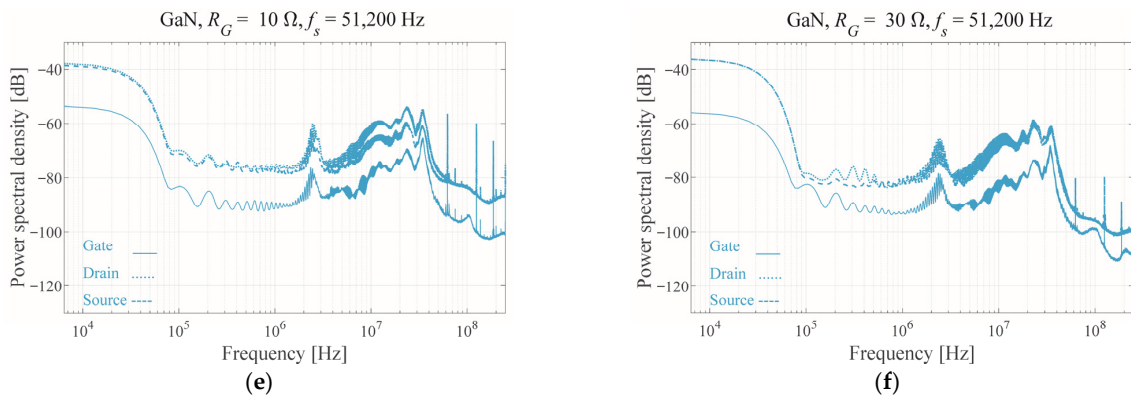


Figure 5. The power spectral density [dB] of the near-field interferences for Si, SiC, and GaN T_1 transistors for $f_s = 51,200$ Hz: (a) Si, $R_G = 10 \Omega$; (b) Si, 30Ω ; (c) SiC, 10Ω ; (d) SiC, 30Ω ; (e) GaN, 10Ω ; (f) GaN, 30Ω .

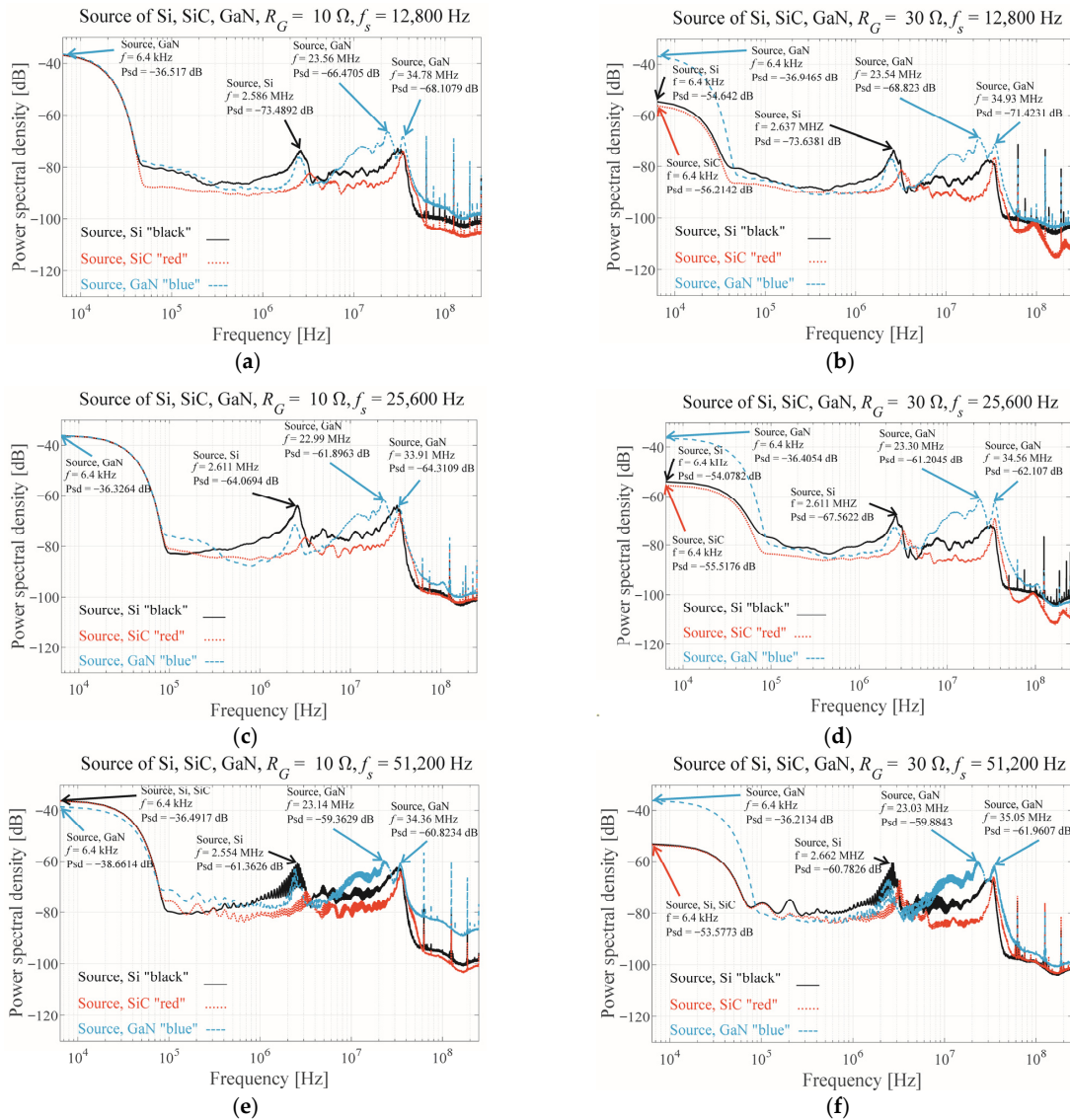
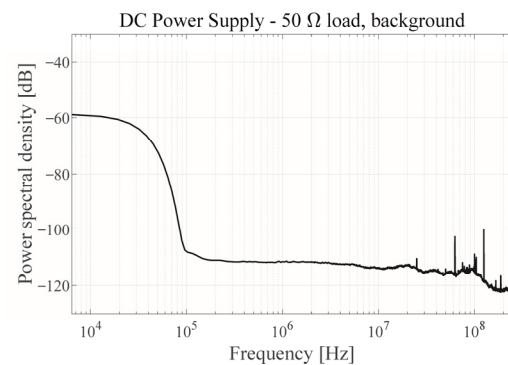


Figure 6. The power spectral density [dB] measured from the T_1 Source of Si, SiC, and GaN transistors for: (a) $R_G = 10 \Omega, f_s = 12,800$; (b) $30 \Omega, 12,800$ Hz; (c) $10 \Omega, 25,600$ Hz; (d) $30 \Omega, 25,600$ Hz; (e) $10 \Omega, 51,200$ Hz; (f) $30 \Omega, 51,200$ Hz.

Table 2. Local maxima of the power spectral density of the near-field interferences (bold—the highest values appointed in Figure 6 for the particular switching frequency and the chosen frequency range).

f_s	Frequency Range for $R_G = 10 \Omega$					Frequency Range for $R_G = 30 \Omega$			
	6400 Hz < $2f_s$	2.45–3.38 MHz	22.99–23.56 MHz	30.45–34.82 MHz	< $2f_s$	2.44–3.24 MHz	23.14–23.54 MHz	29.50–34.97 MHz	
Si	−36.52 dB @6400 Hz	−73.49 dB @ 2.59 MHz	_____	−72.90 dB @30.45 MHz	−54.64 dB @6400 Hz	−73.64 dB @ 2.64 MHz	_____	−77.19 dB @34.97 MHz	
SiC	−36.52 dB @6400 Hz	−82.28 dB @3.38 MHz	_____	−73.8764 dB @34.59 MHz	−56.21 dB @6400	−81.55 dB @3.24 MHz	_____	−76.64 dB @34.95 MHz	
GaN	−36.52 dB @6400 Hz	−76.22 dB @2.47 MHz	−66.47 dB @ 23.56 MHz	−68.11 dB @ 34.78 MHz	−36.95 dB @ 6400 Hz	−77.23 dB @2.44 MHz	−68.83 dB @ 23.54 MHz	−71.42 dB @ 34.93 MHz	
Si	−36.33 dB @6400 Hz	−64.07 dB @ 2.61 MHz	_____	−64.32 dB @32.50 MHz	−54.08 dB @6400 Hz	−67.56 dB @ 2.61 MHz	_____	−71.91 dB @29.50 MHz	
SiC	−36.33 dB @6400 Hz	−76.55 dB @3.19 MHz	_____	−67.48 dB @34.82 MHz	−55.52 dB @6400 Hz	−74.00 dB @3.23 MHz	_____	−69.13 dB @34.39 MHz	
GaN	−36.33 dB @6400 Hz	−71.68 dB @2.45 MHz	−61.90 dB @ 22.99 MHz	−64.31 dB @ 33.91 MHz	−36.41 dB @ 6400 Hz	−72.60 dB @2.52 MHz	−61.20 dB @ 23.30 MHz	−62.11 dB @ 34.56 MHz	
Si	−36.49 dB @6400 Hz	−61.36 dB @ 2.55 MHz	_____	−62.53 dB @31.33 MHz	−53.57 dB @6400 Hz	−60.78 dB @ 2.66 MHz	_____	−67.43 dB @30.71 MHz	
SiC	−36.49 dB @6400 Hz	−71.43 dB @3.17 MHz	_____	−64.11 dB @34.51 MHz	−53.57 dB @6400 Hz	−67.26 dB @3.28 MHz	_____	−65.90 dB @34.23 MHz	
GaN	−38.66 dB @6400 Hz	−62.70 dB @2.46 MHz	−59.36 dB @ 23.14 MHz	−60.82 dB @ 34.36 MHz	−36.41 dB @ 6400 Hz	−66.94 dB @2.47 MHz	−59.88 dB @ 23.03 MHz	−61.96 dB @ 35.05 MHz	

The background power spectral density should be known to prove that the local maxima of transistors' source NFI have no origin from, e.g., DC power supply. So, the NFI was measured on the same load resistor (50Ω) connected directly to the power supply (Figure 7). The background NFI is 5 to 30 dB lower than the measured NFI on the transistor source. The interferences for the frequency range over 50 MHz are from external sources.

**Figure 7.** The power spectral density of the background NFI.

4. Results

The maximum power spectral density of the near-field interferences measured in the experimental model of the voltage source inverter on the source of one of the high transistors in the inverter bridge is presented in Figure 8. It is shown that in the low-frequency range ($f < 2f_s$), the increase (from 10 to 30 Ω) of the serial resistor R_G in the gate circuit seriously reduces the NFI (about 20 dB) and about 0–5 dB in the higher frequency range for Si-MOSFET and SiC-MOSFET; however, it has no (for $f < 2f_s$) or low (for $f > 2$ MHz) influence on the NFI for a GaN transistor. Si and SiC transistor bridges have three maxima of NFI; a GaN transistor bridge has four maxima (the double maxima between 23–35 MHz), probably of its double transistor circuit (the hybrid cascade). SiC transistors cause a lower power spectral density of NFI (1–10 dB) in the frequency range over 2 MHz (Table 2, Figure 8) than Si and GaN transistors. The increase of the switching frequency increases the NFI in this range of frequency.

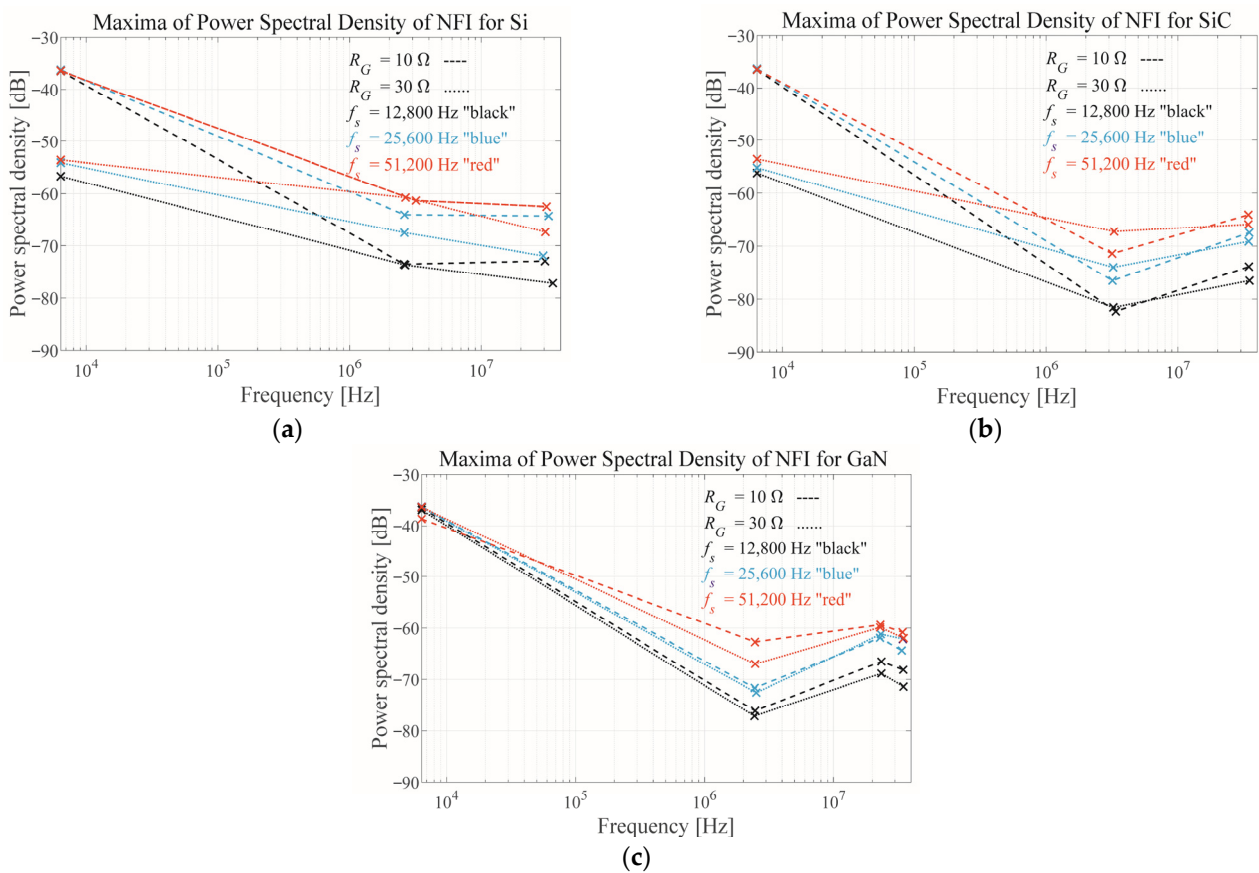


Figure 8. Maxima of the power spectral density of the near-field interferences for 3 technologies of transistors: (a) Si-MOSFET, (b) SiC-MOSFET, (c) GaN cascode device structure.

5. Conclusions

The initial assumption that generally faster transistors cause the higher radiation noise measured using the power spectral density of the near-field interferences on the source of one of the high transistors (where the highest interferences were identified) is false. The lowest radiation noise was for the SiC-MOSFET bridge, lower than for slower Si-MOSFETs. The highest radiation noise was for the GaN cascode device structure and it almost does not depend on the gate R_G resistor. The reason is probably the hybrid (double transistors) structure of the GaN device. It seems the most important influence (concerning the radiation noise) on replacing transistors. The change of Si transistors to SiC transistors decreases the radiation noise of the voltage source inverter; the change to the GaN cascode device structure increases it. Increasing the switching frequency obviously causes the higher radiation noise.

Author Contributions: Conceptualization, Z.R. and K.B.; methodology, Z.R. and K.B.; software, Z.R.; validation, Z.R. and K.B.; formal analysis, Z.R. and K.B.; investigation, Z.R. and K.B.; resources, Z.R. and K.B.; writing—original draft preparation, Z.R.; writing—review and editing, Z.R. and K.B.; visualization, Z.R.; supervision, Z.R. and K.B.; project administration, Z.R. and K.B.; funding acquisition, Z.R. and K.B. All authors have read and agreed to the published version of the manuscript.

Funding: This research was partially supported by the Polish Ministry of Science and Higher Education funding for statutory activities (BK-236/RAu-11/2023).

Data Availability Statement: Not applicable.

Conflicts of Interest: The authors declare no conflict of interest.

References

1. IEC 62040-3:2021; Uninterruptible Power Systems (UPS)—Part 3: Method of Specifying the Performance and Test Requirements. International Electrotechnical Commission (IEC): Geneva, Switzerland, 2021.
2. Jayant Baliga, B. *Fundamentals of Power Semiconductor Devices*, 2nd ed.; Springer International Publishing: Cham, Switzerland, 2019.
3. Siliconix, V. *Power MOSFET Basics: Understanding Gate Charge and Using It to Assess Switching Performance*; Device Application Note AN608A; Vishay Siliconix: San Jose, CA, USA, 2016.
4. Havanur, S. *Power MOSFET Basics: Understanding the Turn-On Process*; Application Note AN850; Vishay Siliconix: San Jose, CA, USA, 2016.
5. Wellmann, P.; Ohtani, N.; Rupp, R. (Eds.) *Wide Bandgap Semiconductors for Power Electronics*; Wiley-VCH: Weinheim, Germany, 2022.
6. Zulauf, G.; Park, S.; Liang, W.; Surakitbovorn, K.N.; Rivas-Davila, J. COSS Losses in 600 V GaN Power Semiconductors in Soft-Switched, High- and Very-High-Frequency Power Converters. *IEEE Trans. Power Electron.* **2018**, *33*, 10748–10763. [[CrossRef](#)]
7. Sun, R.; Lai, J.; Chen, W.; Zhang, B. GaN Power Integration for High Frequency and High Efficiency Power Applications: A Review. *IEEE Access* **2020**, *8*, 15529–15542. [[CrossRef](#)]
8. Millán, J.; Godignon, P.; Perpiñà, X.; Pérez-Tomás, A.; Rebollo, J. A Survey of Wide Bandgap Power Semiconductor Devices. *IEEE Trans. Power Electron.* **2014**, *29*, 2155–2163. [[CrossRef](#)]
9. Bernacki, K.; Rymarski, Z. The Effect of Replacing Si-MOSFETs with WBG Transistors on the Control Loop of Voltage Source Inverters. *Energies* **2022**, *15*, 5316. [[CrossRef](#)]
10. Komurcugil, H. Improved passivity-based control method and its robustness analysis for single-phase uninterruptible power supply inverters. *IET Power Electron.* **2015**, *8*, 1558–1570. [[CrossRef](#)]
11. Ortega, R.; Garcia-Canseco, E. Interconnection and Damping Assignment Passivity-Based Control: A Survey. *Eur. J. Control* **2004**, *10*, 432–450. [[CrossRef](#)]
12. Serra, F.M.; De Angelo, C.H.; Forchetti, D.G. IDA-PBC control of a DC–AC converter for sinusoidal three-phase voltage generation. *Int. J. Electron.* **2016**, *104*, 93–110. [[CrossRef](#)]
13. Rymarski, Z.; Bernacki, K. Different Features of Control Systems for Single-Phase Voltage Source Inverters. *Energies* **2020**, *13*, 4100. [[CrossRef](#)]
14. Rymarski, Z.; Bernacki, K. Technical Limits of Passivity-Based Control Gains for a Single-Phase Voltage Source Inverter. *Energies* **2021**, *14*, 4560. [[CrossRef](#)]
15. Manabe, S. Coefficient diagram method. *IFAC Proc. Vol.* **1998**, *31*, 211–222. [[CrossRef](#)]
16. Manabe, S. Importance of coefficient diagram in polynomial method. In Proceedings of the 42nd IEEE Conference on Decision and Control, Maui, HI, USA, 9–12 December 2003; pp. 3489–3494. [[CrossRef](#)]
17. Hamamci, S.E.; Kaya, I.; Koksall, M. Improving performance for a class of processes using coefficient diagram method. In Proceedings of the 9th Mediterranean Conference on Control and Automation, Dubrovnik, Croatia, 27–29 June 2001; pp. 1–6.
18. Rymarski, Z. The discrete model of the power stage of the voltage source inverter for UPS. *Int. J. Electron.* **2011**, *98*, 1291–1304. [[CrossRef](#)]
19. Coelho, J.P.; Pinho, T.M.; Boaventura-Cunha, J. Controller system design using the coefficient diagram method. *Arab. J. Sci. Eng.* **2016**, *41*, 3663–3681. [[CrossRef](#)]
20. Rymarski, Z. Measuring the real parameters of single-phase voltage source inverters for UPS systems. *Int. J. Electron.* **2017**, *104*, 1020–1033. [[CrossRef](#)]
21. Bernacki, K.; Rymarski, Z.; Dyga, Ł. Selecting the coil core powder material for the output filter of a voltage source inverter. *Electron. Lett.* **2017**, *53*, 1068–1069. [[CrossRef](#)]
22. Rymarski, Z.; Bernacki, K.; Dyga, Ł. Controlled Energy Flow in Z-Source Inverters. *Energies* **2021**, *14*, 7272. [[CrossRef](#)]
23. Liu, T.; Wong, Y.; Shen, Z.J. A Survey on Switching Oscillations in Power Converters. *IEEE J. Emerg. Sel. Top. Power Electron.* **2020**, *8*, 893–908. [[CrossRef](#)]
24. Sadik, D.-P.; Colmenares, J.; Nee, H.-P.; Kostov, K.; Giezendanner, F.; Ranstad, P. Analysis of parasitic elements of SiC power modules with special emphasis on reliability issues. In Proceedings of the 2016 IEEE Applied Power Electronics Conference and Exposition (APEC), Long Beach, CA, USA, 20–24 March 2016; pp. 1018–1023. [[CrossRef](#)]
25. Zeng, Z.; Zhang, X.; Blaabjerg, F.; Miao, L. Impedance-Oriented Transient Instability Modeling of SiC mosfet Intruded by Measurement Probes. *IEEE Trans. Power Electron.* **2020**, *35*, 1866–1881. [[CrossRef](#)]
26. Bernacki, K.; Rymarski, Z. Electromagnetic compatibility of voltage source inverters for uninterruptible power supply system depending on the pulse-width modulation scheme. *IET Power Electron.* **2015**, *8*, 1026–1034. [[CrossRef](#)]
27. Bernacki, K.; Rymarski, Z. Electromagnetic compatibility of impedance source inverters. *Elektron. Ir Elektrotehnika* **2017**, *23*, 55–63. [[CrossRef](#)]
28. Tadakuma, T.; Bisht, P.; Nagahara, T. Experimental approach to identify source of radiation noise over Si and SiC power modules. In Proceedings of the 2018 15th International Conference on Electro Magnetic Interference & Compatibility (INCEMIC), Bengaluru, India, 13–16 November 2018; pp. 1–3. [[CrossRef](#)]

29. Tadakuma, T.; Rogers, M.; Nagahara, T. An Experimental Approach to Identify Source and Cause of Radiation Noise of Inverter Systems and Bare Si Power Chips. In Proceedings of the 2019 IEEE Applied Power Electronics Conference and Exposition (APEC), Anaheim, CA, USA, 17–21 March 2019; pp. 2841–2843. [[CrossRef](#)]
30. Rymarski, Z. Design Method of Single-Phase Inverters for UPS Systems. *Int. J. Electron.* **2009**, *96*, 521–535. [[CrossRef](#)]
31. Smith, S. *Digital Signal Processing: A Practical Guide for Engineers and Scientists*; Elsevier Science: Amsterdam, The Netherlands, 2002; ISBN 9780080477329.
32. Kirilin, R.L.; Bech, M.M.; Trzynadlowski, A.M. Analysis of power and power spectral density in PWM inverters with randomized switching frequency. *IEEE Trans. Ind. Electron.* **2002**, *49*, 486–499. [[CrossRef](#)]

Disclaimer/Publisher’s Note: The statements, opinions and data contained in all publications are solely those of the individual author(s) and contributor(s) and not of MDPI and/or the editor(s). MDPI and/or the editor(s) disclaim responsibility for any injury to people or property resulting from any ideas, methods, instructions or products referred to in the content.